3D Morphological Analysis of the Central Membrane

J. ABREU[1], A. THOREL[1], A. CHESNAUD[1], CH. PEYREGA[2], D. JEULIN[2], F. WILLOT[2], S. PRESTO[3],
1 Mines ParisTech, Center of Materials (CMAT)
2 Mines ParisTech, Center of Mathematical Morphology (CMM)
3 Institute for ENergetics and Interphases, National Research Council, Genova

1. Sample Preparation and Data Acquisition

In order study how we could change the membranes morphology, we decided to produce central membranes with:

- three different porosities: 40%, 50% and 60%
- three different pore formers: polyvinyl butyral, graphite and corn starch
- three different proton conducting to anion conducting volume ratios: 40/60, 50/50 and 60/40

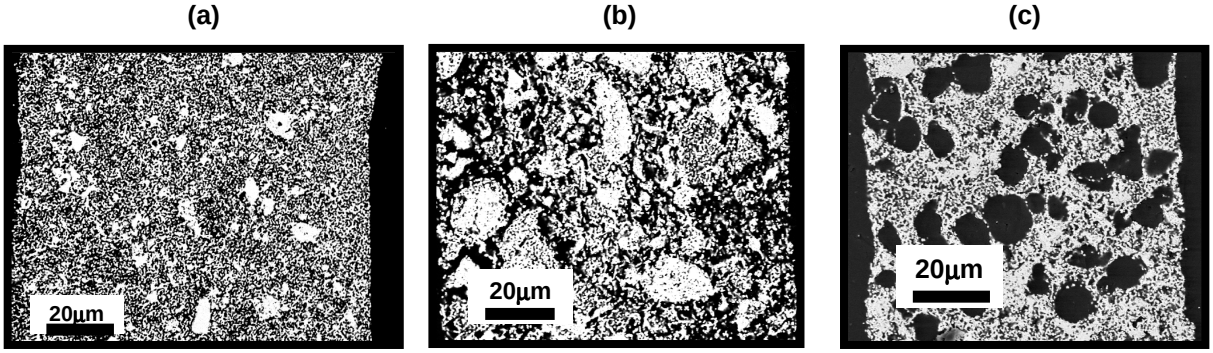

Fig. 1. S.E.M. images of central membranes cross sections for which different pore formers were used: (a) polyvinyl butyral, (b) graphite and (c) corn starch.

Through previous scanning electron microscope analysis (fig.2), we knew that we would have pore sizes between 1 and 15 µm, therefore we would need to work at a resolution of 0,28 µm/pixel which required samples with 300µm x 300µm cross sections in order to not loose important information.
The beam energy chosen was the one for which the two materials would present the highest difference in x-ray absorption. As we can see in Fig. 3, that seemed to occur for energies of about 38keV, however we realised that absorption was too low for such a high energy beam and therefore the quality of the images obtained was not optimal. We worked at 22.5 keV because it showed a better compromise between phase contrast and image quality.

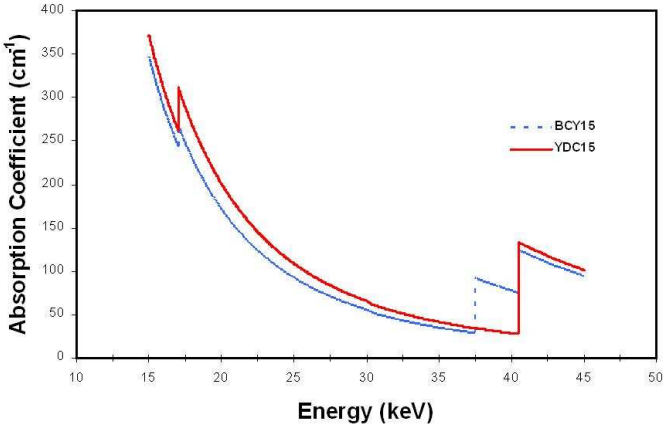

Fig. 2. X-ray absorption coefficient as a function of the beam energy for proton conducting phase (BCY_{15}) and anion conducting phase (YDC_{15}).

Experiments were carried out in 17th and 18th July in the European Synchrotron Radiation Facility in Grenoble, France.

2. Image Processing

2.1. Image Segmentation

After a first analysis of the images obtained it was decided not to work with the samples in which only polyvinyl butyral was used as a pore former because the pores are too small and a correct segmentation of the images was not possible. In the end, data for ten samples was used: five with corn starch and five with graphite as the pore former.

Each of the phases had different x-ray absorptions and therefore each of them presented different grey levels that allowed their segmentation by applying the correct threshold.

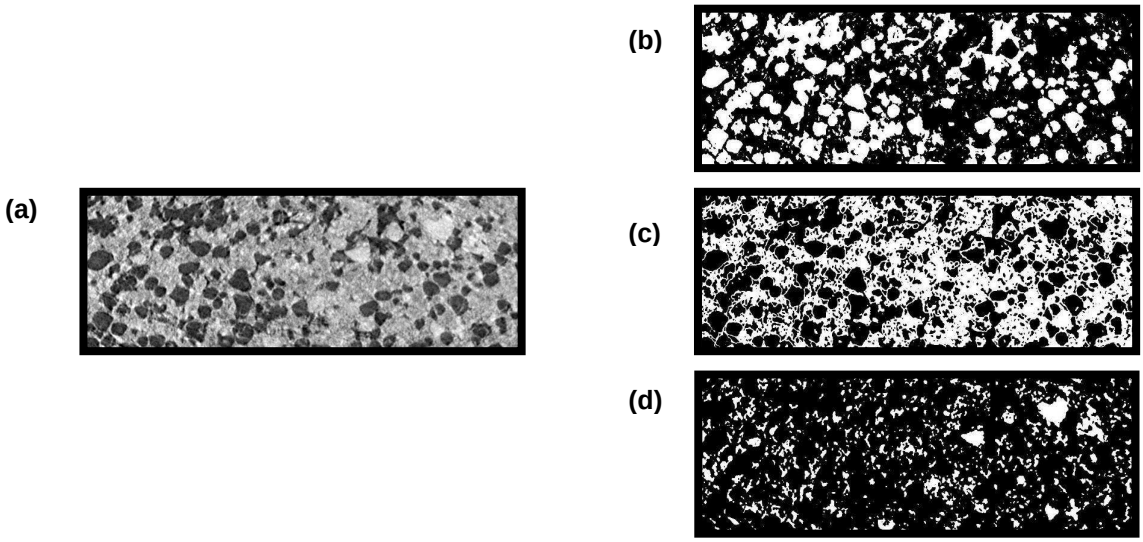

Fig. 3. Image segmentation for a sample with starch as pore former: (a) original image, (b) porosity, (c) anion conducting phase and (d) porosity.

As we expected from the absorption coefficient data (Fig.3), the proton conducting phase is brighter than the anion conducting phase. Porosity was filled with an epoxy resin and appears in the images in black.

We realised, after obtaining this first segmentation, that in the interface between the pores and the brighter phase, voxels with an intermediate grey level were detected and then attributed to the anion conducting phase. This effect created a fake ring around the brighter phase wherever it was in contact with a pore, as one can see in Fig. 4 (a) and (b). The presence of this ring was keeping the proton conducting phase from percolating in the first measurements that were made.

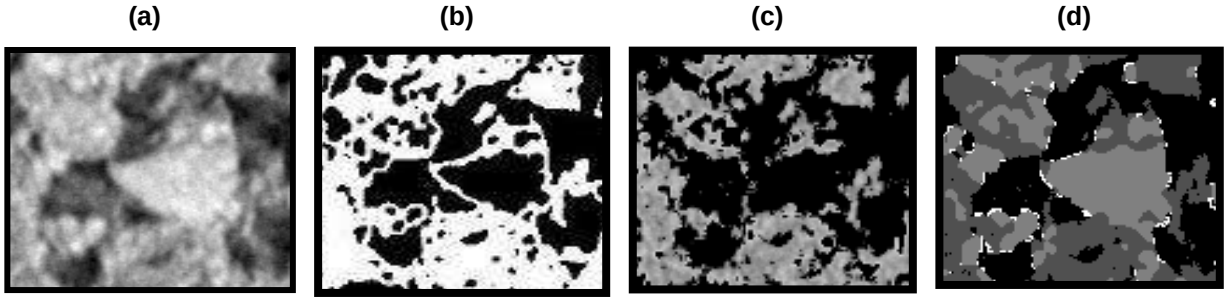

Fig. 4. Detail of an image obtained by x-ray microtomography: (a) original image, (b) first trial for anion conducting phase segmentation, (c) anion conducting phase after image treatment to remove an image detection artefact, (d) final image with the three phases identified.

A sequence of image processing operations was determined in order to eliminate this artefact. The final result is shown in Fig. 4 (c), and as it can be seen the interfaces are noisy and unrealistic due to the former operations. A new sequence of image treatment operations was determined to smooth the surfaces. Each one of the phases was then properly obtained and to each one of them a grey level was attributed (Fig. 4 (d)).

2.2. Active triple phase boundaries extraction

After identifying the three phases for each sample, active triple phase boundaries were extracted. The algorithm used allows identifying the proton and oxygen ion conducting phases in the neighbourhood of porosity. The intersection of the three phases yields the total triple phase boundaries (Fig.6).

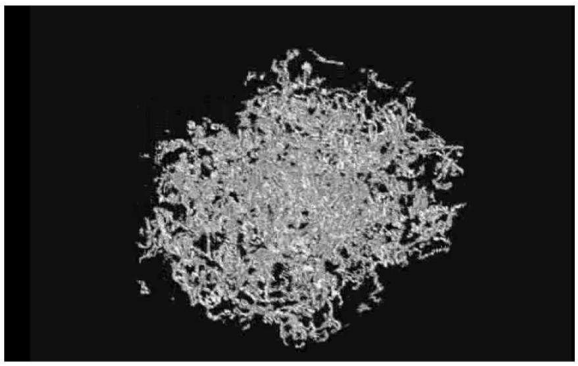

Fig. 5. Total triple phase boundaries for a sample using corn starch as pore former.

The detection of the active *tpb's* required to identify:

- the voxels of proton conducting phase connected to the anode
- the voxels of the anion conducting phase connected to the cathode
- the voxels of porosity connected to the exterior of the fuel cell

These voxels will be the ones reached by a geodesic propagation coming from the surface to which they must be connected. For example all the voxels of the proton conducting phase reached by a geodesic propagation coming from the anode are considered to be connected to it through a path in that phase. The intersection of the three phases gives the segments where the three phases are in contact and each of them percolates to the anode, cathode or exterior of the cell. If we intersect these segments with all the *tpb* previously identified, we obtain the active *tpb*. The percentage of active *tpb* and their length was determined for all of the samples (Table 1).

Table 1. Percentage of active triple phase boundaries and respective length.

sample	% active tpb	active tpb length m/mm^3
A	56	563.3
C	54	606.5
D	39	563.2
H	47	292.0
I	63	441.3
K	52	981.2
L	75	901.4
M	64	909.8
O	58	670.7
R	64	748.2

In an article about 3D reconstruction of an SOFC anode at a higher magnification using SEM-FIB images, James R. Wilson et. al [1] have found 63% of active triple phase boundaries and a specific-volume length of 4,28x10^{3}m/mm^3. Therefore the results obtained can be considered reasonable.

2.3. Phase percolation and tortuosity

After extraction of the three phases and the triple phase boundaries, percolation rates and tortuosities were determined in the *x*, *y* and *z* axis for each one of the phases

The algorithm used to determine percolation applies geodesic propagations into the studied media in the forward and backward directions using a sphere as a structural element. Only the paths that reach the opposite face of the volume in both directions are extracted.

For each one of the voxels belonging to the percolating paths, tortuosity is determined as the ratio of the geodesic distance of the path connecting two opposite faces that passes through that voxel and the Euclidean distance between the two surfaces (fig.7).

(a) 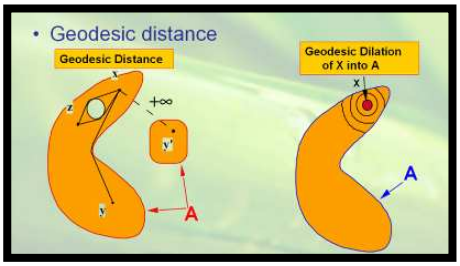

(b) 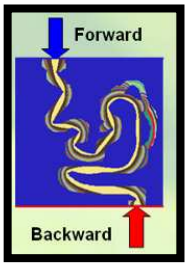

Fig. 6. (a) Definition of geodesic distance and (b) geodesic propagation in a porous medium.

[1] James R. Wilson et al., Three-dimensional reconstruction of a solide oxide fuel-cell anode, Nature Materials, Vol. 5, July 2006

Therefore we obtain not a single value of the tortuosity for a porous structure but a histogram of tortuosities for the voxels that belong to a percolating path.

In Fig.8 and Fig.9 are shown two examples out of the ten samples we analysed.

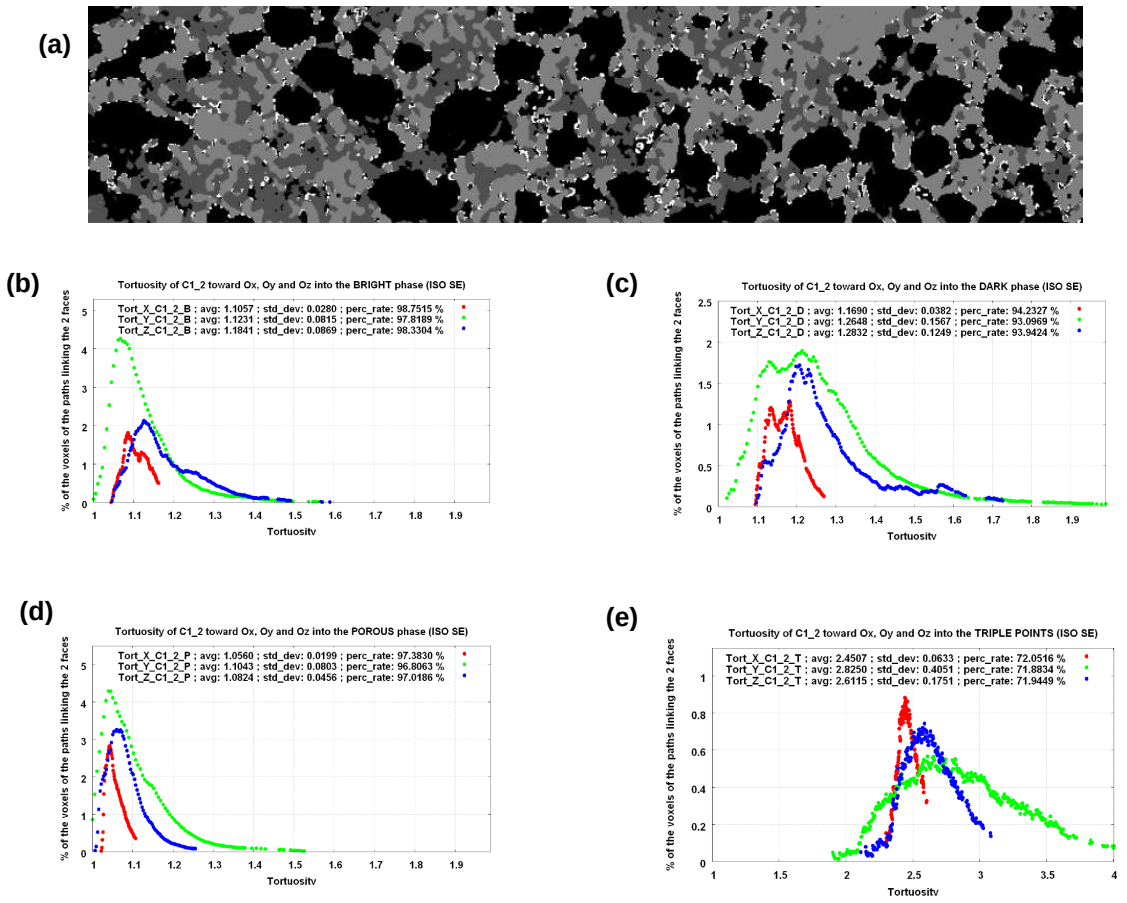

Fig. 7. Results obtained for a sample for which corn starch was used as pore former : (a) 2D cross section with phase segmentation, tortuosity histograms and percolation rates for proton conducting phase (b), anion conducting phase (c), porosity (d) and total triple phase boundaries (e).

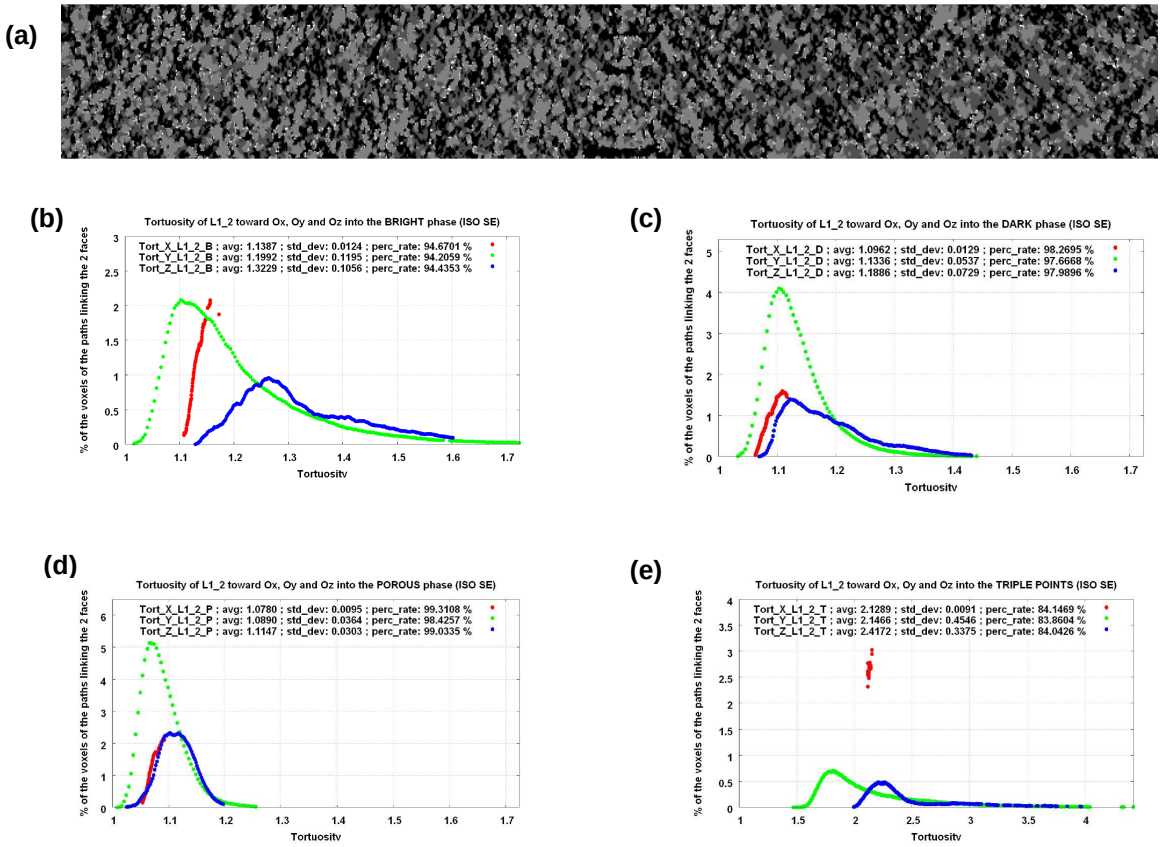

Fig. 8. Results obtained for a sample for which corn starch was used as pore former : (a) 2D cross section with phase segmentation, tortuosity histograms and percolation rates for proton conducting phase (b), anion conducting phase (c), porosity (d) and total triple phase boundaries (e).

Through the results obtained one can conclude that for both types of sample we obtain very high percolating ratios – always above 93% - for the three phases. The percolating paths created are very straight. The tortuosities obtained for each of the phases are very close to one which means that the the path length is very close to the Euclidean distance which is very suitable for charge and mass transportation in the central membrane. On the other hand triple phase boundaries have a tortuosity of about 2,5 which indicates that they are not straight.

3. Prediction of the effective properties of the Central membrane

We developed in Mines ParisTech, Center of Mathematical Morphology (CMM) a software to predict physical properties of materials from images of their microstructure. It is based on the 3D computation of fields from 3D images, based on iterations of FFT transforms.

In the context of the Ideal Cell project, we are able to give the following estimations, for which preliminary results were obtained:

- 3D prediction of the Darcy's permeability tensor by FFT resolution of the Stokes equations
- Conductivity (anionic and protonic)

A first estimation of the Darcy permeability for water of sample shown in Fig.8 was obtained in one direction of propagation of the fluid (Ox). Other directions should be considered, to account for the anisotropy of the porous medium.

The estimated permeability gives
$k = 1.35\ 10^{-10}$,
for a length in cm. This is similar to the permeability of sandstone (in the range 10^{-10}- 10^{-11}).

Similarly, a first estimation of the effective conductivity of each component was obtained for samples C and I, and are given in Table 2. They are obtained for the propagation of current in the same direction as for the flow of water. In this table, we give a relative effective conductivity, that must be multiplied by the absolute conductivity of the corresponding component.

Table 2 Relative effective anionic and cathodic conductivity in the Ox direction

Effective relative conductivity in direction Ox	
Protonic conductivity sample C	0.0551
Anionic conductivity sample C	0.0477
Protonic conductivity sample I	0.0377
Anionic conductivity sample I	0.0530

In a next step, further points will be developed:

- Estimation of the full tensor of permeability and conductivity
- Estimation of the Representative Volume Element for each property
- Validation of the results by comparison to available data, for the input of properties in the macroscopic models

Finally, after calibration, it will be possible to use our approach for application to simulations of models of random microstructures, in order to optimise the effective properties with respect to the end properties of the fuel cell.